Extended investigation of superdeformed bands in ^{151,152}Tb nuclei

J. Robin,[1] Th. Byrski,[1] G. Duchêne,[1] F. A. Beck,[1] D. Curien,[1] N. Dubray,[1] J. Dudek,[1] A. Góźdź,[4] A. Odahara,[1,2] N. Schunck,[1,3] N. Adimi,[5] D. E. Appelbe,[6] P. Bednarczyk,[1,14] A. Bracco,[7] B. Cederwall,[8] S. Courtin,[1] D. M. Cullen,[9] O. Dorvaux,[1] S. Ertück,[9] G. de France,[1] B. Gall,[1] P. Joshi,[1] S. L. King,[9] A. Korichi,[10] K. Lagergren,[8] G. Lo Bianco,[12] S. Leoni,[7] A. Lopez-Martens,[10] S. Lunardi,[11] B. Million,[7] A. Nourredine,[1] E. Pachoud,[1] E. S. Paul,[9] C. Petrache,[12] I. Piqueras,[1] N. Redon,[13] A. Saltarelli,[12] J. Simpson,[6] O. Stezowski,[13] R. Venturelli,[11] J. P. Vivien,[1] and K. Zuber[14]

[1]*Institut de Recherches Subatomiques, UMR 7500, IN2P3-CNRS-ULP, F-67037 Strasbourg Cedex 2, France*
[2]*Nishinippon Institute of Technology, Kanda, Fukuoka 800-03, Japan*
[3]*Department of Physics, University of Surrey, GU2 7XH Guildford, Surrey, United Kingdom*
[4]*Department of Physics, University of Lublin, PL-20031 Lublin, Poland*
[5]*USTHB, Institut de Physique, BP32, El Alia, Bab Ezzouar, 16111 Alger, Algeria*
[6]*CCLRC, Daresbury Laboratory, Daresbury Warrington WA4 4AD, United Kingdom*
[7]*Dipartimento di Fisica dell' Università di Milano and INFN, Sezione di Milano, I-20133 Milano, Italy*
[8]*Royal Institute of Technology, Alba Nova University Center, S-106 91 Stockholm, Sweden*
[9]*Oliver Lodge Laboratory, University of Liverpool, Liverpool L69 7ZE, United Kingdom*
[10]*Centre de Spectrométrie Nucléaire et de Spectrométrie de Masse, IN2P3-CNRS, F-91405 Orsay Campus, France*
[11]*Dipartimento di Fisica dell' Università di Padova and INFN, Sezione di Padova, I-35131 Padova, Italy*
[12]*Dipartimento di Fisica dell' Università di Camerino and INFN, Sezione di Camerino, I-62032 Camerino, Italy*
[13]*Institut de Physique Nucléaire, F-69622 Villeurbanne Cedex, France*
[14]*Institut of Nuclear Physics, PL-31-42 Kraków, Poland*

A detailed study of known and new SD bands in Tb isotopes has been performed with the use of the EUROBALL IV γ-ray array. The high-statistics data set has allowed for the extension of known SD bands at low and high spins by new γ-ray transitions. These transitions, as it turns out, correspond to the rotational frequencies where the principal superdeformed gaps ($Z = 66$, $N = 86$) close giving rise to up- or down-bending mechanisms. This enables to attribute the underlying theoretical configurations with much higher confidence as compared to the previous identifications. Five new SD bands have been discovered, three of them assigned to the ^{152}Tb and the two others to the ^{151}Tb nuclei. Nuclear mean-field calculations have been used to interpret the structure of known SD bands as well as of the new ones in terms of nucleonic configurations.

I. INTRODUCTION

The phenomenon of nuclear superdeformation at high spins has been studied intensively since 1986 when the first superdeformed band in the rare-earth nucleus ^{152}Dy has been found [1]. The single-particle orbital-structure of the nuclear superdeformed states has been relatively simply identified in ^{152}Dy nucleus and in a few of its direct neighbors for the yrast, and for a few low-lying excited bands; for the early evolution of the information on the superdeformed nuclei the reader is referred to the reviews [2]. It is relatively easy to propose the lowest-energy one-particle–one-hole excitations across the big shell gaps leading to lowest-energy excited bands (see the discussion below, and in particular the results in Figs. 3 and 4). However, with increasing excitation there is a large increase in the number of possible particle-hole configurations that differ only little in terms of the p-h excitation energy. Moreover, many of these bands have very similar dynamical moment $\mathcal{J}^{(2)}$ vs rotational frequency, ω, over the whole range of the ω-axis where the corresponding quantities are known experimentally, and thus the identification of the corresponding bands turns out to be ambiguous.

One possible way out of difficulties related to the identification of the bands that are increasingly complicated in

their particle-hole structure can be proposed when studying the typical single-particle Routhian structure around the big SD gaps. In particular, the SD magic gaps are the largest at small rotational frequencies but they close gradually with increasing cranking frequency. It then follows that when the frequencies are sufficiently large, various characteristic crossings among the single-particle Routhians take place that can be used to identify the configurations. However, previous experimental data were often not known sufficiently high in spin and the comparison of the experimental band crossings with those characteristic ones predicted by theory was not possible.

In this paper we present the data on the extended yrast and excited SD bands and also new SD bands in the ^{151,152}Tb nuclei. These data have been obtained in a 17-day run experiment at EUROBALL IV, whose primary goal is the search for discrete linking transitions from the yrast SD band to normal deformed (ND) states in ^{151}Tb nucleus [3]. Consequently, a high statistic data set was obtained. For the eight SD bands already known in ^{151}Tb, several new transitions have been observed at the highest rotational frequencies and a precise determination of many γ-ray energies has been obtained. Five new SD bands have been discovered, two of them have been assigned to ^{151}Tb and three to ^{152}Tb.

Owing to the high-quality experimental data, in this work we were able to identify several critical transitions that indicate several new crossings between the bands and consequently help to clarify a number of open questions related to the interpretation of those bands in terms of the single-particle Routhian structure.

Below we present the new experimental results and the theoretical interpretation of the structure of the measured rotational SD bands based on the cranking mean-field approach with the deformed Woods-Saxon potential according to its 'universal' parametrization, cf. Ref. [4] and references therein. The procedure consists in calculating the $\mathcal{J}^{(2)}$-moments of several hundred bands at several deformation points from the vicinity of the average SD yrast equilibrium deformation. Next, in the process of attributing the theoretically calculated bands to the experimental ones, both the similarity of the corresponding $\mathcal{J}^{(2)}$ vs rotational frequency ω curves as well as the theoretical excitation energies and the experimental population intensities are taken into account as discussed below in detail.

The present paper is organized as follows. An overview of previous studies on the ^{151}Tb nucleus is given in Sec. II. Some details related to the experimental setup are presented in Sec. III and the results, including some examples of the experimental spectra are presented in Sec. IV (the corresponding Tables of the obtained transition energies are given in the Appendix). The results from calculations results and the comparison with experiment are given in Sec. VI.

II. ^{151}TB NUCLEUS : AN OVERVIEW

The level scheme of ^{151}Tb has been determined to very high spins and excitation energies [5]. The theoretical interpretation of its decay pattern associated with the normal- (as opposed to super)deformation indicates a gradual transition from a nearly spherical- to an oblate-shape, the calculated oblate deformation increasing slowly with excitation energy and spin from $\beta \approx -0.05$ up to $\beta \approx -0.20$ [5].

The corresponding noncollective transitions are slower as compared to the two other groups of transitions seen typically in the nuclei in this mass range: the collective rotational bands associated with the moderate quadrupole deformation but characterized, according to the calculations, by a relatively strong triaxiality, and the superdeformed transitions.

The nucleus ^{151}Tb has been one of the first nuclei in the $A \sim 150$ mass region in which many SD bands involving proton- and neutron-holes in the SD gaps $Z = 66$ and $N = 86$ have been observed [6,7]. Moreover the first observation of identical superdeformed bands was made in this nucleus [8]. In the following we concentrate on the SD bands, their properties and interpretation.

III. EXPERIMENTAL CONDITIONS

The terbium isotopes were produced via the ^{130}Te (^{27}Al, xn) reaction at the beam energy of 155 MeV. A stack of two self-supporting ^{130}Te, each $\sim$500 μg cm^{-2} thick was used with the ^{27}Al beam provided by the Vivitron accelerator of the Institut de Recherches Subatomiques of Strasbourg, France.

The γ-ray decays of the residual nuclei were measured using the Euroball IV array which consisted of 30 tapered detectors (forward quadrant), 26 clover detectors (around 90°), and 15 cluster detectors (backward angles). Associated to an inner ball of BGO detectors (210 crystals), they formed a device of 164 groups of 'equivalent' detectors in terms of solid angle and efficiency—allowing us to measure the multiplicity and the sum energy of γ-rays emitted in a nuclear reaction.

A coincidence fold selection of at least six unsuppressed (four suppressed) Ge detectors and of at least ten BGO ball elements firing was required for selecting high-multiplicity events. The relative yields of the main evaporation channels $5n$, $6n$, and $7n$ are 13%, 77%, and 10%, respectively. After Compton suppression a total yield of 8.7×10^9 four-fold and higher-fold events was obtained, leading to a mean multiplicity value of 5. In the analysis of the data set a nonspiked database [9] has been used. The search for new SD bands in Tb isotopes was carried out using an automatic search code [10] which requires three of four gates to be satisfied before identifying regular sequences of γ-ray transitions.

IV. RESULTS

In the present data set, due to the very high statistics and an improved peak-to-background ratio, a total of 15 SD bands has been observed. Apart from the eight bands previously assigned to ^{151}Tb and two SD bands assigned to ^{152}Tb, [11], five new SD bands were clearly identified.

The search for new SD structures in these Tb nuclei turned out to be a delicate task since several factors contributed to technical and/or practical difficulties:

  (i) The overall weak population of the SD bands;
 (ii) Competition with low-lying SD bands that are therefore populated with stronger *relative* intensity;
(iii) The presence, within one single nucleus, of many SD bands with similar $\mathcal{J}^{(2)}$ behavior and overlapping over long stretches of rotational frequencies;
(iv) The presence of some SD bands with no regular behavior of their $\mathcal{J}^{(2)}$ moments.

It then follows that considerable efforts were necessary for the extension of experimental knowledge of well established SD bands up to the highest observable frequencies, especially in the feeding region close to the fission limit.

A careful, complementary analysis has been performed using a new background subtraction method [12]. By using background spectra very representative of those in coincidence with SD bands we succeeded in keeping maximum statistics in SD peaks.

The γ-ray transition energies of the ten SD bands, labeled from 1 to 10 in the ^{151}Tb case, and 1 to 5 in that of ^{152}Tb, are listed in Tables III, IV, V, and VI in the Appendix. The new SD bands are labeled 9 and 10 and 1 to 3 in ^{151}Tb and ^{152}Tb, respectively. The new γ-ray energies observed in this experiment and also the energies of all the band members already known in ^{151,152}Tb nuclei are included in the tables.

The spectra of the new SD bands are displayed in Fig. 1. The highest energy parts of the ^{151}Tb(1–8) bands, where the new transitions are clearly seen, are presented in Fig. 2.
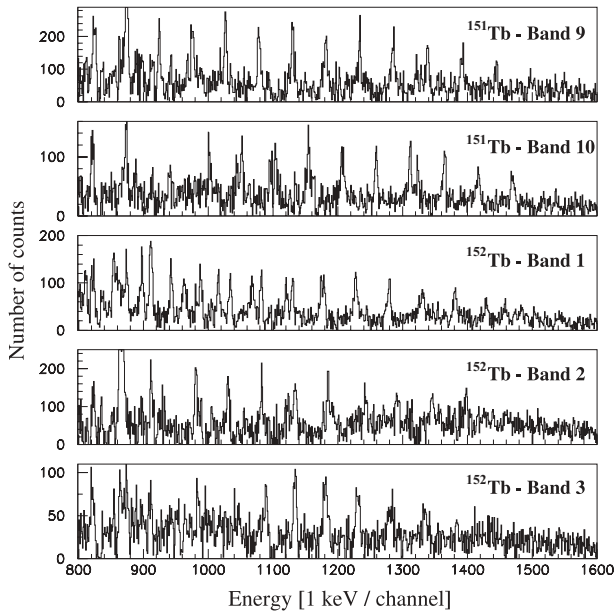
FIG. 1. Triple-gated spectra showing the new excited SD bands in the nuclei ^{151}Tb and ^{152}Tb.

V. CALCULATIONS AND COMPARISON WITH EXPERIMENT

Structures of all SD bands in ^{151,152}Tb nuclei have been analyzed using the Woods-Saxon cranking approach with the 'universal' parameter set, (see Ref. [4], and references therein). Detailed calculations show that the equilibrium deformations depend somewhat on the particle-hole configuration of the particular SD band in question. With increasing rotational frequency, most of the nuclei shrink, i.e., the corresponding quadrupole deformation β_2 decreases. A slight modification in
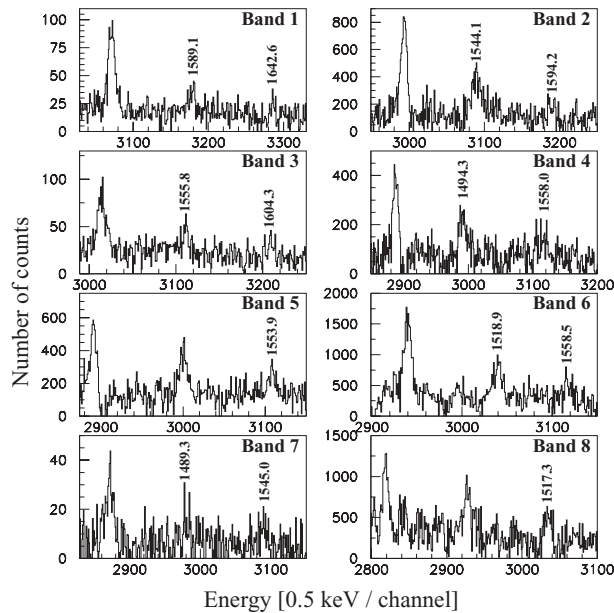

FIG. 2. The highest energy part of double and triple-gated spectra showing the new γ-ray transitions observed in ^{151}Tb(1–8). The new transitions are labeled by their energy.
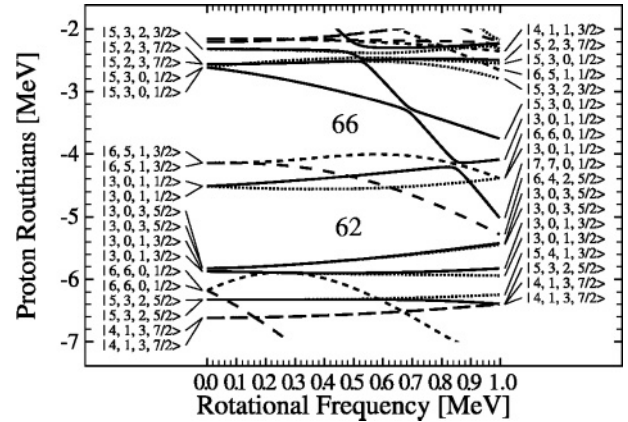

FIG. 3. Single-proton energy levels obtained with the Woods-Saxon potential as functions of rotational frequency for deformation parameters characteristic of the yrast SD band in ^{152}Dy and its closest neighbors. We use the standard notation for the parity, π, and for the signature exponent α. In particular, the solid lines represent the orbitals with $(\pi, \alpha) = (-, -1/2)$; the dotted lines those with $(\pi, \alpha) = (-, +1/2)$; the short-dashed lines those with $(\pi, \alpha) = (+, +1/2)$; the long-dashed lines those with $(\pi, \alpha) = (+, -1/2)$. Deformation parameters: $\beta_2 = 0.61$, $\beta_4 = 0.11$.

the hexadecapole deformation β_4 accompanies this evolution, but these are essentially all the systematic shape changes that are induced by rotation. In particular the triaxiality parameter γ remains close to zero for most of the bands in the nuclei that are close neighbors of the SD doubly-magic ^{152}Dy nucleus.

In the following calculations, we used the shapes and shape evolution for the even-even nuclei as tabulated in Ref. [13]. A typical average deformation corresponding to the ^{152}Dy nucleus has been selected for the Routhian diagrams in Figs. 3 and 4 that will be used as the reference when discussing the particle-hole excitations analyzed below.

We use the usual notation related to the occupation of the special, intruder orbitals, i.e., those characterized by $N = 6$ for the protons and $N = 7$ for the neutrons. For instance, configuration corresponding to the occupation of two proton-intruder levels and three neutron-intruder levels
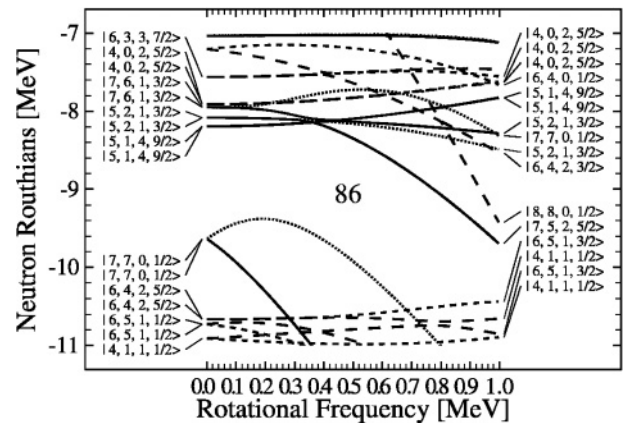

FIG. 4. Single-neutron energy levels obtained with the Woods-Saxon potential as functions of rotational frequency; for further details see caption Fig. 3.

will be denoted $\pi^2\nu^3$. For the detailed reference related to the single-particle routhians, the Nilsson labels shown in Figs. 3 and 4 will be used.

According to the so-far unexplained 'moment-of-inertia anomaly' discussed in Ref. [14], the $\mathcal{J}^{(2)}$ moments calculated using the Woods-Saxon mean-field potential are on the average $\sim$10% larger than the experimental values (here we address the unambigous conclusions based on the comparison of the regular curves, i.e., not the ones possibly 'contaminated' by the band crossings). The self-consistent Hartree-Fock results produce a similar anomaly, with the deviations that are slightly smaller, 7–8 %. Since this systematic deviation applies in a similar fashion to all the bands studied, it has been suggested [14] to introduce a reduction factor $f = 0.9$; the corresponding common renormalization applied to all the calculated moments facilitates the legibility of comparisons (illustrations) and has been applied also below.

A. Proton configurations

A quadrupole moment of 17.2 eb, [15], has been attributed to the ^{151}Tb yrast SD band. This measurement confirms clearly the superdeformed character of the underlying nuclear configuration. According to the accepted interpretation, its structure is based on the $\pi 6^3\nu 7^2$ configuration in terms of high-N intruder orbitals. The corresponding explicit Nilsson labels can be read from Fig. 3: for the protons they are $\pi\,|660\,1/2\rangle_{\alpha=\pm1/2}$, and $\pi|651\,3/2\rangle_{\alpha=-1/2}$. Similarly, the neutron intruder labels can be read from Fig. 4: they are $\nu|770\,1/2\rangle_{\alpha=\pm1/2}$.

The labels 2, 3, and 4 associated with the first three excited bands reflect the decreasing relative population intensity. The interpretation of the related configurations accepted by several authors is that of the lowest-lying proton particle-hole excitations (cf., e.g., [14] and references quoted therein). Here the structures of bands ^{151}Tb(2–4) have been reanalyzed taking into account a more complete experimental information.

The experimental and theoretical dynamical moments $\mathcal{J}^{(2)}$ of the SD-bands (1–4) are plotted in Fig. 5 as functions of rotational frequency. As this work has allowed for the identification of new γ-ray transitions at very high frequencies and a higher precision in the measurement of the SD γ-ray transition-energies with weak intensities, we were able to extract accurate values of dynamical moments and to observe their behavior approaching closer to the fission limit. Modifications in the smooth variation of $\mathcal{J}^{(2)}$ at very high ω should reflect the crossings of the bands predicted by theory. These crossings appear at the frequencies corresponding to the closing up the magic gaps at the highest frequency limit as discussed above. Observation of such effects in the experiment imposes new constraints on the possible particle-hole configurations underlying the description of those SD bands.

Band ^{151}Tb(1). The experimental results for the yrast band, ^{151}Tb(1), indicate that the $\mathcal{J}^{(2)}$ moments show a regular decrease with frequency up to the highest observed values of $\hbar\omega\sim0.8$ MeV with, nevertheless, some fluctuations at the end of the band. The theoretical results for $\mathcal{J}^{(2)}$ moments based on the $\pi 6^3\nu 7^2$ intruder configuration indicate a strong discontinuity at a very high rotational frequency ($\hbar\omega\sim0.80$ MeV) caused by the interaction between the
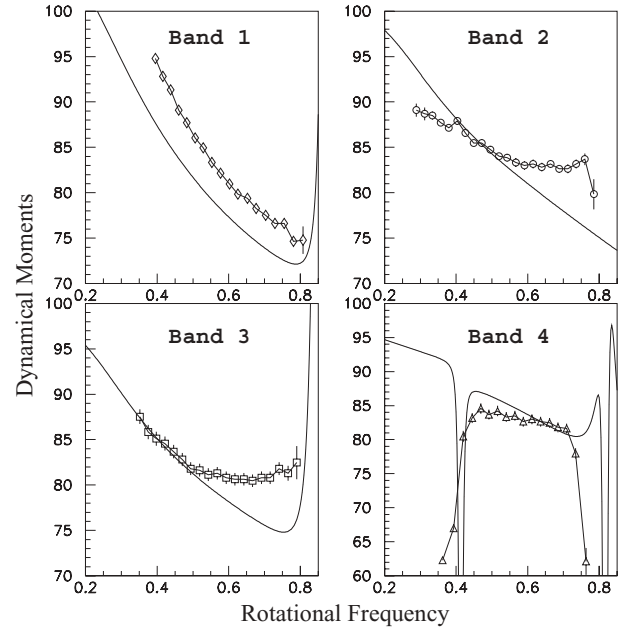

FIG. 5. Experimental and calculated dynamical moments $\mathcal{J}^{(2)}$ ($\hbar^2$ MeV^{-1}) as functions of rotational frequency (MeV) for the proton excited SD bands in ^{151}Tb. The underlying particle-hole configurations are displayed in Table I.

$\pi\,|301\,1/2\rangle_{\alpha=-1/2}$ and $\pi|770\,1/2\rangle_{\alpha=-1/2}$ orbitals, visible from Fig. 3. Unfortunately, no higher frequencies than $\hbar\omega=0.8$ MeV have been observed, suggesting either a possible closeness of the fission limit or that the strong crossing of the bands does indeed take place at the predicted frequency in which case an extra loss of population intensity could be expected. This is because in such a case the closeness of the two crossing bands implies a competition in terms of a given feeding flux that is in such a case split into two, with half the intensity each.

Band ^{151}Tb(2). The measured intensity of the first excited SD band, ^{151}Tb(2), relative to the yrast band is $\approx$29(3)%. This strongly suggests that at the high spin window where this band is populated it corresponds most likely to the second excited Routhian. From inspection of Figs. 3 and 4 it follows that there are several possible candidate-configurations possible. In Ref. [14] it has been proposed that the underlying structure corresponds to the $\pi\,|301\,1/2\rangle_{\alpha=-1/2}$ proton hole in the yrast SD band of ^{152}Dy. In that case, according to Fig. 3 no manifestation of the crossing between the above mentioned orbitals $\pi\,|301\,1/2\rangle_{\alpha=-1/2}$ and $\pi|770\,1/2\rangle_{\alpha=-1/2}$ is expected.

Band ^{151}Tb(3). This band is populated with a relative intensity of 24(2)%, a value very close to the one for band ^{151}Tb(2). This similarity suggests that the two bands could be signature partners, provided that the underlying single-particle Routhian-partners do not manifest any dramatic signature splitting. Concerning the $\mathcal{J}^{(2)}$ moment of ^{151}Tb(3) with the suggested $\pi 6^4(|651\,3/2\rangle_{\alpha=+1/2})^{-1}\nu 7^2$ configuration [14] a smooth rise is clearly identified above $\hbar\omega\sim0.65$ MeV; this pattern is explained by the expected crossing just mentioned [cf. also Fig. (3)].

Band ^{151}Tb(4). Band 4 relative intensity is 13(2)%. In Ref. [14] it has been shown that experimental results for bands

TABLE I. Configurations of all SD bands in ^{151}Tb deduced from [14] and this work.

SD Bands	Excitation	Configuration	Similarity
1	yrast	$\pi 6^3 \otimes \nu 7^2$	
2	proton	$\pi 6^4(\lvert 301\,1/2\rangle_{\alpha=-1/2})^{-1} \otimes \nu 7^2$	^{152}Dy yrast
3	proton	$\pi 6^4(\lvert 651\,3/2\rangle_{\alpha=+1/2})^{-1} \otimes \nu 7^2$	^{152}Dy yrast
4	proton	$\pi 6^4(\lvert 301\,1/2\rangle_{\alpha=+1/2})^{-1}$	^{152}Dy yrast
	neutron	$\nu 7^2(\lvert 411\,1/2\rangle_{\alpha=-1/2})^{-1}(\lvert 761\,3/2\rangle_{\alpha=+1/2})^{+1}$	
5	neutron	$\pi 6^3 \otimes \nu 7^1(\lvert 402\,5/2\rangle_{\alpha=+1/2})^{+1}$	^{150}Tb yrast
6	neutron	$\pi 6^3 \otimes \nu 7^1(\lvert 402\,5/2\rangle_{\alpha=-1/2})^{+1}$	^{150}Tb yrast
7	neutron	$\pi 6^3 \otimes \nu 7^1(\lvert 521\,3/2\rangle_{\alpha=-1/2})^{+1}$	^{150}Tb yrast
8	neutron	$\pi 6^3 \otimes \nu 7^1(\lvert 521\,3/2\rangle_{\alpha=+1/2})^{+1}$	^{150}Tb yrast
9	neutron	$\pi 6^3 \otimes \nu 7^1(\lvert 514\,9/2\rangle_{\alpha=-1/2})^{+1}$	^{150}Tb yrast
10	neutron	$\pi 6^3 \otimes \nu 7^1(\lvert 514\,9/2\rangle_{\alpha=+1/2})^{+1}$	^{150}Tb yrast

2 and 4 agree well with configurations based on exciting either of the signature partners of the $\pi \lvert 301\,1/2\rangle_{\alpha=\pm1/2}$ orbitals into the $\pi \lvert 651\,1/2\rangle_{\alpha=+1/2}$. However, the new data allow extending the observed frequency range for band ^{151}Tb(4) and therefore to identify the well pronounced down-sloping in $\mathcal{J}^{(2)}$ moment, at low and high rotational frequencies, which was not reproduced with previous calculations. Taking into account that the intensity of band 4 is about half the one of band 2, a new configuration assignment is proposed based on the excitation of the $\pi \lvert 301\,3/2\rangle_{\alpha=+1/2}$ orbital into the $\pi \lvert 651\,3/2\rangle_{\alpha=+1/2}$ one and the excitation of the $\nu \lvert 411\,1/2\rangle_{\alpha=-1/2}$ orbital into the $\nu \lvert 761\,3/2\rangle_{\alpha=+1/2}$ one. The characteristic down-sloping of the theoretical $\mathcal{J}^{(2)}$ moments with increasing frequency, at $\hbar\omega \sim 0.75$ MeV is caused by the crossing of the neutron orbitals $\nu \lvert 761\,3/2\rangle_{\alpha=+1/2}$ and $\nu \lvert 521\,3/2\rangle_{\alpha=+1/2}$. Similarly, the strong down-sloping of dynamical moments with decreasing frequency is caused by the emptied down-bending $\nu \lvert 411\,1/2\rangle_{\alpha=-1/2}$ neutron orbital [for details of the configurations cf. Table I]. Another interpretation is also proposed below when discussing band 6 configuration.

B. Neutron configurations

The experimental results for bands ^{151}Tb(5–8) indicating a strong correlation with the yrast sequence of the isotope ^{150}Tb have been related to neutron particle-hole excitations [14]. The previous calculations indicate that several neutron particle-hole excitations give a very similar dependence of the dynamical moments as function of rotational frequency. These are excitations from the $\nu \lvert 770\,1/2\rangle_{\alpha=+1/2}$ orbital to either of the $\nu \lvert 402\,5/2\rangle$, $\nu \lvert 521\,3/2\rangle$ or $\nu \lvert 514\,9/2\rangle$ orbitals. Therefore only the more likely explanations have been proposed (cf. Table I).

Bands ^{151}Tb(5,6). The intensities of bands 5 and 6 relative to the yrast SD band are 13(3)% and 14(3)%, respectively. Concerning the $\mathcal{J}^{(2)}$ moments of the ^{151}Tb(5,6) signature partner bands their previously observed degeneracy ceases at very high frequencies as a strongly marked upbend alters the smooth behavior of $\mathcal{J}^{(2)}$ for one component (Fig. 6). Calculations based on an excitation from the $\nu \lvert 770\,1/2\rangle_{\alpha=+1/2}$ orbital to the $\nu \lvert 402\,5/2\rangle_{\alpha=\pm1/2}$ orbital and for deformation parameters $\beta_2 = 0.59$, $\beta_4 = 0.11$ agree comparably well with the experimental data for bands 5 and 6 (Fig. 6). Band 5 corresponds to a neutron excitation from the $\nu \lvert 770\,1/2\rangle$ state

to the the $\nu \lvert 402\,5/2\rangle_{\alpha=+1/2}$ orbital while band 6 involves the signature partner of the last orbital. This component interacts strongly with the $\nu \lvert 633\,7/2\rangle_{\alpha=-1/2}$ and $\nu \lvert 642\,3/2\rangle_{\alpha=-1/2}$ orbitals at frequencies $\hbar\omega \geqslant 0.75$ MeV. Thus, those new data have allowed us to fix (in the frame of these calculations) the configurations associated to bands ^{151}Tb(5, 6).

The case of band 4 with two down-bending $\mathcal{J}^{(2)}$ structures at low ($\hbar\omega \sim 0.4$ MeV) and high ($\hbar\omega \sim 0.7$ MeV) frequencies can be related to the two up-bending $\mathcal{J}^{(2)}$ structures (the lowest being expected and the highest clearly seen) of band 6. This may reflect an accidental degeneracy in excitation energy, supported by the fact that those two bands have similar intensities leading to similar excitation energy. Moreover, making the assumption that those two bands interact at a spin of $63.5\hbar$ (based on the calculations made in Ref. [16]), their different $\mathcal{J}^{(2)}$ behavior means that they also interact again at the spin $31.5\hbar$, which is in good agreement with the
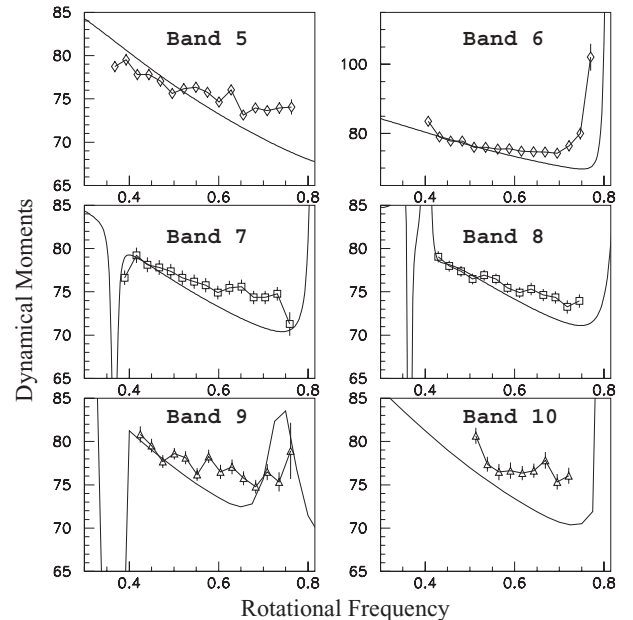

FIG. 6. Experimental and calculated dynamical moments $\mathcal{J}^{(2)}$ ($\hbar^2$ MeV^{-1}) as functions of rotational frequency (MeV) for the neutron excited SD bands in ^{151}Tb.

rotational frequencies where the up- and down-bendings occur. On this hypothesis, we should be able to observe crossover gamma-rays at the interaction points. Unfortunately, the two possible crossings occur at the very bottom and top of both bands hindering the chance to see any transitions of band 6 in band 4 spectrum, and vice versa. In addition, the interband transitions for the high frequency crossing would be very weak as they are located in the SD bands feeding region. At low frequency these lines are drowned in the spectrum by a high density of intense normal-deformed transitions. In conclusion with the present statistics, there is no way to confirm experimentally the hypothesis of a double SD band crossing between bands 4 and 6.

Bands $^{151}Tb(7,8)$. The $\mathcal{J}^{(2)}$ moments for bands 7 and 8 do not exhibit marked discontinuities except the presence of weak oscillations above $\hbar\omega \sim 0.65$ MeV. Among the remaining neutron configurations mentioned above, we have associated the $\nu[521]3/2(\alpha = \pm 1/2)$ to these bands as in Ref. [14] but at different deformation parameters ($\beta_2 = 0.61$ and $\beta_4 = 0.11$). The comparison of calculated results obtained for the $\nu |770\ 1/2\rangle_{\alpha=+1/2} \rightarrow \nu |521\ 3/2\rangle_{\alpha=\pm1/2}$ excitation with experimental ones is presented in Fig. 6. A pronounced upbend is expected at $\hbar\omega \sim 0.8$ MeV, but not observed in these data as the last experimental point corresponds to $\hbar\omega < 0.79$ MeV. The measured relative intensity of bands 7 and 8, 10(3) and 10(2)% respectively, agree with a configuration assignment of signature partners with no sizable signature splitting.

Bands $^{151}Tb(9,10)$. The two new $^{151}Tb(9, 10)$ bands are the less populated with relative intensities of 8(2) and 7(2)%, respectively. They are characterized by a $\mathcal{J}^{(2)}$ moment (Fig. 6) similar to those of bands having the $\pi 6^3 \nu 7^1$ high-N intruder configurations: $^{149}Gd(3)$, $^{150}Tb(1)$, $^{151}Tb(5, 6, 7, 8)$. The γ-ray transition energies of $^{151}Tb(9, 10)$ bands resemble those of a signature-partner pair. The corresponding similarity is remarkably well maintained over the full observed frequency range. The similarity between the $\mathcal{J}^{(2)}$ moments in $^{150}Tb(1)$ and in $^{151}Tb(9, 10)$ suggest that the intruder neutron Routhian $\nu |770\ 1/2\rangle_{\alpha=+1/2}$ is not occupied in the related configurations and that the corresponding neutron particle-hole excitation involves a low-lying orbital with a small $\mathcal{J}^{(2)}$ contribution. Theoretical predictions favour the neutron excitation $\nu |770\ 1/2\rangle_{\alpha=+1/2} \rightarrow |514\ 9/2\rangle_{\alpha=\pm1/2}$; according to this, at high rotational frequencies ($\hbar\omega \geqslant 0.6$ MeV), the crossing of the $\nu |514\ 9/2\rangle_{\alpha=-1/2}$ and $\nu |521\ 3/2\rangle_{\alpha=-1/2}$ is followed by that of the $\nu |514\ 9/2\rangle_{\alpha=+1/2}$ and $\nu |521\ 3/2\rangle_{\alpha=+1/2}$ (Fig. 4). Taking into account the similarity between the calculated curves and the experimental ones, the $\pi 6^3 \nu 7^1 (|770\ 1/2\rangle_{\alpha=+1/2})^{-1}(|514\ 9/2\rangle_{\alpha=-1/2})^{+1}$ and $\pi 6^3 \nu 7^1 (|770\ 1/2\rangle_{\alpha=+1/2})^{-1}(|514\ 9/2\rangle_{\alpha=+1/2})^{+1}$ configurations have been assigned to bands 9 and 10, respectively.

C. New excited SD bands in ^{152}Tb

Three new SD bands were clearly identified and assigned to ^{152}Tb. Bands 1 and 2, with γ-ray energies very close to those of the strongly populated $^{151}Tb(1)$ band were not easily observed. The γ-ray transition energies of bands 1 to 5 are
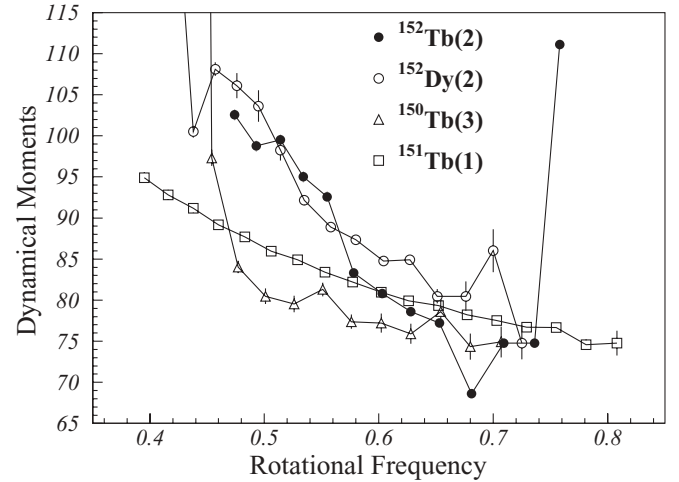

FIG. 7. Experimental dynamical moments $\mathcal{J}^{(2)}$ ($\hbar^2$ MeV^{-1}) as a function of rotational frequency [MeV] for the SD bands $^{152}Tb(2)$, $^{152}Dy(2)$, $^{150}Tb(3)$, and $^{151}Tb(1)$.

listed in Table VI. The intensity of ^{152}Tb yrast SD band relative to the $5n$ channel have been measured to be 1.6%. In Table VI, the bands intensity are given in percent of the intensity of the yrast band.

The corresponding experimental $\mathcal{J}^{(2)}$ moments are plotted in Fig. 7 as a functions of rotational frequency. In contrast to already known $^{152}Tb(4,5)$ bands with $\mathcal{J}^{(2)}$ moments having a regular behavior, the $\mathcal{J}^{(2)}$ moments of $^{152}Tb(1, 2, 3)$ bands display significant irregularities and therefore comparison with the similar possibly existing in the literature $\mathcal{J}^{(2)}$ forms of behavior was not easy.

Band $^{152}Tb(1)$. In this analysis the $\pi 6^3 \nu 7^3$ high-N intruder configuration has been assigned to $^{152}Tb(1)$ as the most probable one and we propose it as the yrast SD band in ^{152}Tb. To reinforce this statement, the band $^{152}Tb(1)$ has actually the highest intensity of all bands found in this nucleus. The comparison between theoretical results and experimental ones for $^{152}Tb(1, 2, 3)$ bands is illustrated in Fig. 8.

Band $^{152}Tb(2)$. The γ-ray energies of $^{152}Tb(2)$ band are very close to the energies of the $^{152}Dy(2)$ band over a large part of the observed energy range. Their $\mathcal{J}^{(2)}$ moments show the same steeply uprising slope below $\hbar\omega \approx 0.55$ MeV (Fig. 7). Above this frequency, all the bands in question [$^{152}Tb(2)$, $^{152}Dy(2)$, and $^{150}Tb(3)$] manifest the slope similar to that of $^{151}Tb(1)$. The $\mathcal{J}^{(2)}$ moment of $^{150}Tb(3)$ presents similar features, especially a pronounced increase in $\mathcal{J}^{(2)}$ below $\hbar\omega \approx 0.50$ MeV.

In Ref. [20] the $\pi 6^4 \pi 7^1 (|301\ 1/2\rangle)^{-1} \nu 7^2$ configuration has been assigned to $^{152}Dy(2)$ as the most likely interpretation. The increase in $\mathcal{J}^{(2)}$ below $\hbar\omega = 0.5$ MeV has been attributed to the crossing between the $\pi |770\ 1/2\rangle$ and $\pi |330\ 1/2\rangle$ orbitals. For the $^{150}Tb(3)$ band the $\pi 6^3 \nu 7^2$ high-N intruder configuration has been proposed, coupled to a hole in either the $|654\ 5/2\rangle$ or $|651\ 1/2\rangle$ neutron orbitals [17]. The sharp rise of $\mathcal{J}^{(2)}$ at $\hbar\omega \approx 0.45$ MeV was associated to a $N = 7$ quasineutron paired band crossing. Our experiment results for band 2 agree rather well with calculation for a configuration based on two excitations, one neutron from the $\nu |402\ 5/2\rangle_{\alpha=+1/2}$

TABLE II. Configurations of SD bands in ^{152}Tb deduced from [14] and this work.

SD Bands	Excitation	Configuration	Similarity
1	yrast	$\pi 6^3 \otimes \nu 7^3$	
2	proton	$\pi 6^3 (\lvert 301\,1/2\rangle_{\alpha=-1/2})^{-1} (\lvert 530\,1/2\rangle_{\alpha=-1/2})^{+1}$	^{152}Dy(2)
	neutron	$\nu 7^2 (\lvert 402\,5/2\rangle_{\alpha=+1/2})^{-1} (\lvert 521\,3/2\rangle_{\alpha=+1/2})^{+1}$	
3	neutron	$\pi 6^3 \otimes \nu 7^2 (\lvert 402\,5/2\rangle_{\alpha=-1/2})^{-1} (\lvert 761\,3/2\rangle_{\alpha=-1/2})^{+1}$	^{150}Tb yrast
4	neutron	$\pi 6^3 \otimes \nu 7^2 (\lvert 402\,5/2\rangle_{\alpha=+1/2})^{+1}$	^{151}Tb yrast
5	neutron	$\pi 6^3 \otimes \nu 7^2 (\lvert 402\,5/2\rangle_{\alpha=-1/2})^{+1}$	^{151}Tb yrast

orbital into the $\nu \lvert 521\,3/2\rangle_{\alpha=+1/2}$ state and a proton from the $\pi \lvert 301\,1/2\rangle_{\alpha=-1/2}$ orbital into the $\pi \lvert 530\,1/2\rangle_{\alpha=-1/2}$. The neutron excitation has a relatively low-cost in energy due to a high-density level of orbitals. The discontinuity in $\mathcal{J}^{(2)}$ observed above $\hbar\omega \approx 0.7$ MeV result from the crossing of the $\pi 7^1$ and $\pi \lvert 530\,1/2\rangle_{\alpha=-1/2}$ orbitals.

Band ^{152}*Tb(3)*. According to our calculations, band ^{152}Tb(3) is suggested to be based on a neutron excitation from the $\nu \lvert 402\,5/2\rangle_{\alpha=-1/2}$ orbital into the $\nu \lvert 761\,3/2\rangle_{\alpha=-1/2}$ one. The discontinuity observed at $\hbar\omega \approx 0.6$ MeV in the $\mathcal{J}^{(2)}$ moment is caused by the interaction between non intruder orbitals $\nu \lvert 402\,5/2\rangle_{\alpha=-1/2}$ and $\nu \lvert 642\,3/2\rangle_{\alpha=-1/2}$.

Bands ^{152}*Tb(4,5)*. These two signature partner bands have already been observed in this nucleus with $\mathcal{J}^{(2)}$ moments very similar to that of ^{151}Tb(1) [11]. With the observation of new γ-ray transitions in the feeding region, this similarity is maintained up to the highest observed rotational frequency. These experimental results agree rather well with calculations for the configuration $\pi 6^3 \nu 7^2 (\lvert 402\,5/2\rangle_{\alpha=\pm1/2})^{+1}$ (Fig. 8). Table II summarizes the configuration assignments for various SD bands observed in ^{152}Tb isotopes.

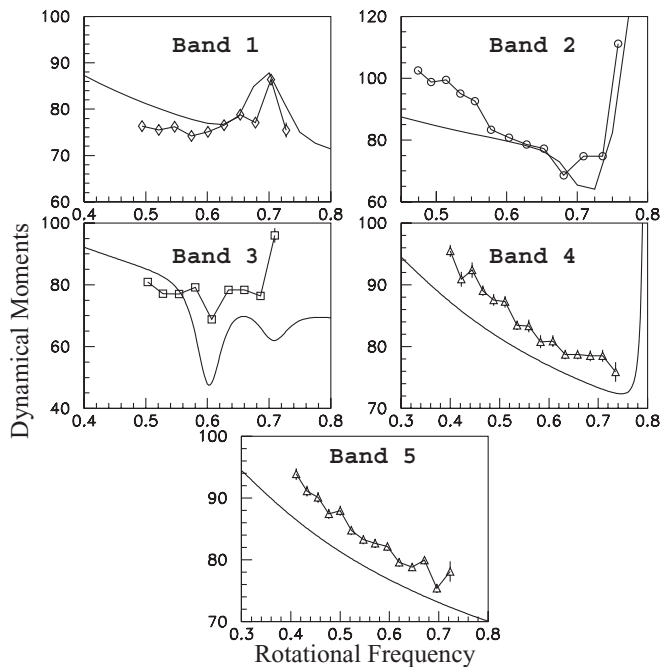FIG. 8. Experimental and calculated dynamical moments $\mathcal{J}^{(2)}$ ($\hbar^2$ MeV^{-1}) as functions of rotational frequency (MeV) for the SD bands in ^{152}Tb.

VI. CONCLUSIONS

An extensive study of SD bands in ^{151,152}Tb isotopes has been performed, allowing the for a reinterpretation of nucleonic configuration assignments on the basis of comparison between experimental results and universal-parametrization Woods-Saxon mean-field calculations. Five new SD bands have been discovered, raising the number of known bands to ten and five, in ^{151}Tb and ^{152}Tb isotopes, respectively. Among those, two bands [^{151}Tb(4) and ^{152}Tb(2)] have been interpreted as a two particle-hole excitations (one neutron plus one proton) in order to reproduce their dynamical moments of inertia.

In the present experiment the experimental data were obtained during the 17 day run with the EUROBALL IV array. The obtained high quality spectra allowed to find the transitions whose presence made it possible to eliminate a number of competing single-nucleonic configurations and at the same time propose nearly unambiguous interpretation in terms of the others. Our experiment shows clearly that the high-precision experimental data are crucial for determining the underlying single-particle structure and cross-testing the microscopic nuclear high-spin theories in an efficient way. This is because the numerous crossings among the single-particle Routhians that appear at the very high frequency limit where the superdeformed magic gaps finally close, offer a (complicated but often unique and powerful) scheme of up- and or down-bending structures that distinguish clearly among the numerous bands whose dynamical moments otherwise behave in a very regular manner.

The results obtained here indicate that the most powerful present day detection arrays are at the limit of the detection capacities needed to perform the conclusive nuclear high-spin structure determination. It becomes clear that with an increase of the detection efficiency by about a factor of 4 (cf. AGATA and GRETA), a few days running time experiments of the type performed here will become of extreme importance in the future with the beam-time limitations becoming prohibitively scarce.

APPENDIX

In this appendix we have summarized the experimental results obtained so far on the superdeformed bands in ^{151,152}Tb nuclei. These results, in the form of the transition energies are given in Tables III–VI.

TABLE III. Transition energies (keV) and statistical uncertainties for the SD bands in ^{151}Tb. The asterisk * indicates new transitions or old ones with an enhanced precision. The band intensities are given in percent of the intensity of the yrast band. The error bars include the statistical fluctuations and the dispersion of the band intensity along the SD band plateau.

Band 1 100(2)%	Band 2 29(3)%	Band 3 24(3)%	Band 4 13(2)%
	556.2(2)*		
	601.1(3)		
	646.2(2)		
	691.4(1)	681.2(3)	
	737.0(1)	726.9(3)	691.7(3)*
768.6(1)	782.9(1)	773.5(3)	755.9(3)*
810.8(1)	828.4(2)	820.5(3)	815.6(4)
853.9(1)	874.6(1)	867.8(3)	865.3(3)
897.7(1)	921.4(1)	915.6(3)	913.4(3)
942.6(1)	968.2(2)	963.9(3)	960.7(3)
988.2(1)	1015.4(1)	1012.8(3)	1008.5(3)
1034.7(1)	1063.0(1)	1061.8(3)	1056.0(3)
1081.8(1)	1110.7(2)	1111.1(3)	1104.0(3)
1129.8(1)	1158.7(2)	1160.3(3)	1151.9(3)
1178.5(1)	1206.9(2)	1209.8(3)	1200.3(3)
1227.9(1)	1255.0(2)	1259.4(3)	1248.5(3)
1278.0(1)	1303.3(2)	1309.0(3)	1296.9(3)
1328.4(1)	1351.4(1)	1358.7(3)	1345.4(3)
1379.5(1)	1399.8(2)	1408.2(3)	1394.3(3)
1431.1(1)	1448.2(2)	1457.7(3)	1443.3(3)
1483.3(1)	1496.3(2)	1506.6(3)	1494.6(4)*
1535.5(2)	1544.1(3)*	1555.8(4)*	(1559(2))*
1589.1(4)*	1594.2(1.0)*	1604.3(1.0)*	
1642.6(1.0)*			

TABLE IV. Similar to that in Table III but for Bands 5–8.

Band 5 13(3)%	Band 6 14(3)%	Band 7 10(3)%	Band 8 10(2)%
709.8(3)	790.6(3)	754.3(4)	
760.6(3)	838.5(3)	806.5(4)	831.8(3)*
810.9(3)	889.1(3)	857.0(4)	882.4(3)
862.3(3)	940.5(3)	908.2(4)	933.7(3)
913.7(3)	991.9(3)	959.6(4)	985.4(3)
965.6(3)	1044.5(3)	1011.3(4)	1037.7(3)
1018.5(3)	1097.1(3)	1063.5(4)	1089.7(3)
1071.0(3)	1150.1(3)	1116.0(4)	1142.0(3)
1123.4(3)	1203.0(3)	1168.8(4)	1195.0(3)
1176.2(3)	1256.4(3)	1222.2(4)	1248.4(3)
1229.8(3)	1309.9(3)	1275.2(4)	1301.5(4)
1282.4(3)	1363.5(3)	1328.1(4)	1355.1(3)
1337.1(3)	1417.3(1.0)	1381.9(4)	1408.9(4)
1391.2(3)	1469.6(4)	1435.7(4)*	1463.5(4)
1445.5(4)	1519.6(1.0)*	1489.2(4)*	1517.6(4)*
1499.6(4)	1558.8(1.1)*	(1545.3(1.0))*	
1553.6(5)*			

TABLE V. Similar to that in Table III, but for Bands 9 and 10.

Band 9 8(2)%	Band 10 7(2)%
824.4(5)	
873.9(3)	
924.2(4)	
975.7(3)	
1026.6(3)	1001.6(4)
1077.8(4)	1051.2(4)
1130.3(3)	1102.9(4)
1181.4(4)	1155.2(5)
1233.7(4)	1207.4(4)
1285.6(4)	1259.8(4)
1338.4(4)	1312.0(4)
1391.9(4)	1363.4(5)
1444.2(5)	1416.5(4)
1497.3(6)	1469.1(5)
1548(2)	

TABLE VI. Transition energies (keV) and statistical uncertainties for the SD bands in ^{152}Tb. The asterisk * indicates new transitions or old ones with an enhanced precision. The band intensities are given relatively to the 5n reaction channel population. The error bars include the statistical fluctuations and the dispersion of the band intensity along the SD band plateau.

Band 1 1.6%	Band 2 1.2%	Band 3 0.6%	Band 4 0.6%	Band 5 0.5%
			779.5(3)*	801.0(3)
			821.4(3)*	843.6(3)
			865.4(5)*	887.5(3)
	927.5(5)		908.7(3)	931.9(3)
	966.5(5)		953.6(4)	977.7(3)
962.8(3)	1007.0(5)	980.9(3)	999.3(4)	1023.1(3)
1015.2(3)	1047.2(3)	1030.4(3)	1045.2(3)*	1070.3(3)
1068.1(3)	1089.3(3)	1082.2(3)	1093.1(3)*	1118.4(3)
1120.6(3)	1132.5(3)	1134.1(3)	1141.1(5)	1166.8(3)*
1174.5(3)	1180.5(3)	1184.7(3)	1190.6(4)*	1215.4(3)
1227.8(3)	1230.0(3)	1242.8(3)	1240.1(4)	1265.7(3)*
1280.0(3)	1280.9(3)	1293.9(3)	1290.9(3)	1316.4(3)*
1330.8(3)	1332.7(3)	1345.0(3)	1341.7(4)	1366.4(3)
1382.7(3)	1391.0(5)	1397.3(3)	1392.7(4)*	1419.5(4)*
1429.0(6)	1444.5(1.0)	1439.0(1.0)	1443.6(5)*	1470.7(1.0)*
1482.0(1.0)	1498.0(1.0)		1496.3(1.0)*	
	15340(1.0)			

[1] P. J. Twin *et al.*, Phys. Rev. Lett. **57**, 811 (1986).

[2] R. V. F. Janssens and T. L. Khoo, Annu. Rev. Nucl. Part. Sci. **41**, 321 (1991); J. F. Sharpey-Schafer, Prog. Part. Nucl. Phys. **28**, 187 (1992); J. Dudek, Prog. Part. Nucl. Phys. **28**, 131 (1992); C. Baktash, B. Haas, and W. Nazarewicz, Annu. Rev. Nucl. Part. Sci. **45**, 485 (1995).

[3] J. Robin *et al.* (to be published).

[4] S. Ćwiok, J. Dudek, W. Nazarewicz, J. Skalski, and T. Werner, Comput. Phys. Commun. **46**, 379 (1987).

[5] C. M. Petrache *et al.*, Nucl. Phys. **A579**, 285 (1994).

[6] B. Kharraja *et al.*, Phys. Lett. **B341**, 268 (1995).

[7] G. de France *et al.*, Phys. Lett. **B331**, 290 (1994).

[8] T. Byrski *et al.*, Phys. Rev. Lett. **64**, 1650 (1990).

[9] O. Stezowski, Ch. Finck, and D. Prévost, Nucl. Instrum. Methods A **424**, 552 (1999).

[10] S. Flibotte, U. J. Hüttmeier, P. Bednarczyk, G. de France, B. Haas, P. Romain, Ch. Theisen, J. P. Vivien, and J. Zen, Nucl. Instrum. Methods A **320**, 325 (1992).

[11] B. Kharraja, Ph.D. thesis, Université Louis Pasteur, Strasbourg I, France (1994).

[12] J. Robin, Nucl. Instrum. Methods A **555**, 282 (2005).

[13] T. R. Werner and J. Dudek, At. Data Nucl. Data Tables **50**, 179 (1992); **59**, 1 (1995).

[14] N. El Aouad *et al.*, Nucl. Phys. **A676**, 155 (2000).

[15] Ch. Finck *et al.*, Eur. Phys. J. A **2**, 123 (1998).

[16] I. Ragnarsson *et al.*, Nucl. Phys. **A557**, 167c (1993).

[17] P. Fallon *et al.*, Phys. Rev. C **52**, 93 (1995).

[18] N. Kintz *et al.*, Proceedings of the XXXVIII International Winter Meeting on Nuclear Physics, Bormio, 2000, pp. 77–82.

[19] S. Flibotte *et al.*, Phys. Rev. Lett. **71**, 4299 (1993).

[20] P. J. Dagnall *et al.*, Phys. Lett. **B335**, 313 (1994).

[21] I. Hamamoto and B. R. Mottelson, Phys. Scr. T **56**, R1 (1995); Phys. Lett. **B333**, 294 (1994).

[22] J. Dudek, A. Góźdź, and D. Rosły, Acta Phys. Pol. B **32**, 2625 (2002) (freely available at http://th-www.if.uj.edu.pl/acta/).

[23] W. D. Luo, A. Bouguettoucha, J. Dobaczewski, J. Dudek, and X. Li, Phys. Rev. C **52**, 2989 (1995); J. Dudek, J. Dobaczewski, W. Luo, A. Bouguettoucha, and X. Li, Proc. Int. Workshop on Physics with Recoil Separators and Detector Arrays, New Delhi, India 1995.

[24] D. S. Haslip, S. Flibotte, C. E. Svensson, and J. C. Waddington, Phys. Rev. C **58**, R1893 (1998).

[25] Y. Sun, J. Y. Zhang, and M. Guidry, Phys. Rev. Lett. **75**, 3398 (1995).